To be published in: Proceedings of the 18th European Biomass Conference & Exhibition, May 2010, Lyon, France,
ETA-Renewable Energies (Ed.), Italy

OPTIMISATION OF BIOMASS GRATE FURNACES WITH A NEW 3D PACKED BED COMBUSTION MODEL - ON EXAMPLE OF A SMALL-SCALE UNDERFEED STOKER FURNACE

Ramin Mehrabian[1,2,*], Robert Scharler[1,2,3], Alexander Weissinger[4], Ingwald Obernberger[1,2,3]
[1]BIOENERGY 2020+ GmbH, Inffeldgasse 21b, 8010 Graz, Austria
Tel.: +43 (0)316 8739232; Fax: +43 (0)316 8739202; E-mail: ramin.mehrabian@bioenergy2020.eu
[2]Institute for Process and Particle Engineering, Graz University of Technology, Inffeldgasse 21b, A-8010 Graz, Austria
[3]BIOS BIOENERGIESYSTEME GmbH, Inffeldgasse 21b, A-8010 Graz, Austria
[4]KWB - Kraft und Wärme aus Biomasse GmbH, Industriestrasse 235, A-8321 St. Margarethen, Austria

ABSTRACT: The design and optimisation of a biomass grate furnace requires accurate and efficient models for the combustion process on the grate as well as the turbulent reactive flow in the combustion chamber. Computational Fluid Dynamics (CFD) have been successfully applied for gas phase combustion. However, no numerical models for the biomass packed bed combustion, which can be used as engineering design tools, are commercially available at present. This paper presents an innovative 3D CFD model for biomass packed bed combustion consisting of an Euler-Granular model for hydrodynamics of gas-particle multiphase flow and a thermally thin particle model for combustion of biomass particles. Modelling the particle trajectories and the thermal conversion of each particle in the bed constitutes the simulation of the entire bed combustion. The simulation of a small-scale underfeed stoker furnace of KWB has been successfully performed by the application of the new packed bed combustion model. The positions of the drying, pyrolysis and char burnout zones in the fuel bed as well as the temperature distribution among the particles seem to be plausible and could be confirmed by observations. Furthermore, a good qualitative agreement concerning the flue gas temperatures measured by thermocouples at different positions in the combustion chamber, and CO emissions measured at boiler outlet could be achieved. The new packed bed model provides the advantages of considering the release profiles of species and energy from the fuel bed close to reality and enables to consider the chemical compositions, size and physical properties of the fuel particles as well as the influence of primary air distribution and grate motion on the particle trajectories.
Keywords: biomass, combustion, fixed bed, CFD, modelling.

1 INTRUDUCTION AND OBJECTIVES

CFD simulation techniques are an efficient tool for the design and optimisation of biomass grate furnaces. They have demonstrated to be valuable to predict the flow and the gas phase combustion in furnaces [1-4]. However, at present there is a lack of reasonably accurate and computationally efficient simulation tools for packed bed biomass combustion.

The main problems encountered in modelling biomass packed bed combustion are the hydrodynamics of the gas-solid multiphase flow and thermal conversion of the biomass particles. There are various simulation methods applicable to the dense gas-solid multiphase flows (granular flows). Generally they can be classified into two approaches: the discrete element methods (DEM) based on the molecular dynamics and the continuum mechanics methods or two-fluid model (TFM) based on the assumption that the gas and particulate phases form two inter-penetrating continua [5].

The discrete element method is fully based on the Lagrangian framework, i.e. the motion of each particle is defined by classical Newtonian mechanics and contact mechanics of deformation. The particle-particle collision is modelled by the soft sphere method [6] or hard sphere method [7]. In general, discrete models are powerful and they are able to predict the rotation and velocity of each particle. Moreover, they allow the investigation of the effect of individual physical particle properties in the granular flow. The limiting parameter in the DEM is the number of particles. Hence, in most cases, the calculation time is too high for industrial scale systems.

The Euler/Euler two-fluid model assumes that the particulate phase behaves as a fluid. Therefore, the continuity and momentum equations with jump conditions for phase interfaces are solved for both gas and particulate phases. In this approach all the particles are assumed to be identical, specified by their mean diameter and density. Therefore handling a poly-disperse system, i.e. a system with different particle sizes, requires several solid phases corresponding to the number of particle diameter classes. Hjertager reported a quadratical increase of computational effort with the number of phases [8]. Additionally, the modelling of particle-particle collisions in this approach is rather complicated. It has been implemented in the momentum equation of solid phase by the viscosity and normal stress tensor of the solid phase. There are several correlations for the solid viscosity term and the solid normal stress tensor [9-14]. They have been driven by making an analogy between the particle-particle collisions and the kinetic theory of gases [15]. The concept of granular temperature is defined to represent the kinetic energy of random particle fluctuations around their mean velocities. A conservation energy equation is formulated for this kinetic fluctuation energy in which the kinetic energy is produced by shear and fluid turbulence and dissipated by inelastic collisions and interaction with the fluid. The collisions between the particles are assumed to be a function of this kinetic fluctuation energy. The capability of the TFM for simulation of granular systems has been proven by its numerous applications, see [16] and its references.

In the present work the commercial CFD software, ANSYS FLUENT 12, has been utilised to simulate the hydrodynamics of the packed bed granular flow. Among the available gas-solid multiphase models in ANSYS FLUENT the Euler-Granular model has been selected because it is based on the kinetic theory of granular flows and allows the consideration of inter-particle interactions which are of key importance in modelling of packed beds. This model has been successfully used for predicting the hydrodynamic behaviour of a bubbling fluidised bed [17-19]. In this study the Euler-Granular

model was applied for an underfeed stoker grate furnace for the first time.

As already mentioned, the thermal conversion of the biomass particles is another challenge in modelling of biomass packed bed combustion. A realistic approach is to consider the packed bed as an ensemble of finite representative particles, where each of these particles undergoes a sequence of processes such as heat-up, drying, pyrolysis, and oxidation. The Euler-Granular model opted for tracing the particle trajectories in the packed bed does not allow considering these processes for each individual particle. Therefore, the modelling of particles thermal conversion was performed by the ANSYS FLUENT discrete phase model (DPM). Although the DPM is not suitable for particle tracking under packed bed conditions, because it ignores the volume of particles and particle-particle collisions, its combustible particle model provides a powerful tool to simulate the thermal conversion of each biomass particle and in turn the entire packed bed.

In this study a 3D packed bed model based on the combination of Euler-Granular model for predicting the hydrodynamics of the packed bed and the discrete phase model for the thermal conversion of the packed bed is presented. Then the model was applied for the first time to simulate the fixed bed combustion in an underfeed stoker furnace.

2 METHODOLOGY

Packed bed modelling was divided into two parts, hydrodynamics of the packed bed multiphase flow, and thermal conversion of the biomass particles. The Euler-Granular model was selected to simulate the former and the later was predicted by the discrete phase model (DPM). In order to combine these two models in ANSYS FLUENT a simulation with non-reacting flow based on the Euler-Granular model with appropriate granular viscosity (empirically determined) was performed and the simulated velocity field of the granular phase was stored as user defined memory (UDM). Then these data were used to prescribe the particle velocities in the DPM simulation by means of a user defined function (UDF).

In the DPM simulation, as a first approach, the particles are assumed to be thermally thin, i.e. temperature is uniform inside the particles. Moreover, the convection and radiation heat transfer between the particle-gas as well as particle-particle radiation is considered. The standard DPM drying and pyrolysis models describe the release rates of the water vapour and volatile components. The standard DPM diffusion limited char burnout model was modified, in order to consider the effect of particle-gas relative velocity on the rate of particle heterogeneous oxidation reaction. The turbulent reactive flow in the combustion chamber above the packed bed was described by the following models: the Realizable k-ε model for turbulence; the Eddy Dissipation Model with modified Magnussen constants [1] for turbulence-chemistry interaction, a global 4-step mechanism considering volatiles, CH_4, CO, CO_2, H_2, H_2O, and O_2 for gas phase combustion, and the Discrete Ordinate Model for radiation.

In the next sections the governing equations for both parts of the packed bed model are explained.

2.1 Hydrodynamics of the packed bed

The Euler-Granular model treats the gas-solid multiphase flow as interpenetrating continua. It incorporates the concept of the volume fraction. The volume fraction represents the space occupied by each phase and they are assumed to be continuous functions of space and time and their sum is equal to one:

$$\sum_{i=1}^{n} \alpha_i = 1 \tag{1}$$

Conservation equations for solid and gas phase are derived to obtain a set of equations. They have similar structure for both phases because of the same Eulerian treatment. The mass balance for phase k yields

$$\frac{\partial}{\partial t}\left(\alpha_k \rho_k\right) + \nabla \cdot \left(\alpha_k \rho_k \vec{u}_k\right) = \sum_{\substack{i=g,s \\ i \neq k}} \left(\dot{m}_{ik} - \dot{m}_{ki}\right) \tag{2}$$

where ρ is the density $\left[kg.m^{-3}\right]$ and $\vec{u}$ is the velocity vector $\left[m.s^{-1}\right]$. $\dot{m}_{ik}$ characterises the mass transfer $\left[kg.s^{-1}.m^{-3}\right]$ from the ith to the kth phase and $\dot{m}_{ki}$ characterises the mass transfer from the kth to the ith phase.

The momentum conservation equation for gas and solid phase are:

$$\begin{aligned}\frac{\partial}{\partial t}\left(\alpha_g \rho_g \vec{u}_g\right) + \nabla \cdot \left(\alpha_g \rho_g \vec{u}_g \vec{u}_g\right) = \\ -\alpha_g \nabla p + \nabla \cdot \bar{\tau}_g + \alpha_g \rho_g \vec{g} \\ + \left(K_{gs} \cdot \left(\vec{u}_s - \vec{u}_g\right) + \dot{m}_{sg}\vec{u}_s - \dot{m}_{gs}\vec{u}_g\right)\end{aligned} \tag{3}$$

$$\begin{aligned}\frac{\partial}{\partial t}\left(\alpha_s \rho_s \vec{u}_s\right) + \nabla \cdot \left(\alpha_s \rho_s \vec{u}_s \vec{u}_s\right) = \\ -\alpha_s \nabla p - \nabla p_s + \nabla \cdot \bar{\tau}_s + \alpha_s \rho_s \vec{g} \\ + \left(K_{gs}\left(\vec{u}_g - \vec{u}_s\right) + \dot{m}_{gs}\vec{u}_g - \dot{m}_{sg}\vec{u}_s\right)\end{aligned} \tag{4}$$

where K_{gs} is the interphase momentum exchange coefficient $\left[kg.s^{-1}.m^{-3}\right]$.

The constitutive equations are required to close the governing equations.

- Gas phase Newtonian viscous stress tensor:

$$\bar{\tau}_g = \alpha_g \mu_g \left[\left(\nabla \vec{u}_g + \nabla \vec{u}_g^{\,T}\right) - \frac{2}{3}\nabla \cdot \vec{u}_g \bar{I}\right] \tag{5}$$

where μ_g is the molecular viscosity $\left[N.s.m^{-2}\right]$, $\bar{I}$ is the identity matrix, and the second term on the right hand side is for the effect of compressibility.

- Solid phase stress tensor:

$$\bar{\tau}_s = \alpha_s \mu_s (\nabla \vec{u}_s + \nabla \vec{u}_s^{\,T}) + \alpha_s \left(\lambda_s - \frac{2}{3}\mu_s\right)\nabla \cdot \vec{u}_s \bar{I} \tag{6}$$

where μ_s is the solid shear viscosity $\left[N.s.m^{-2}\right]$ and λ_s is the solid bulk viscosity $\left[N.s.m^{-2}\right]$.

- Solid phase pressure:

$$p_s = \alpha_s \rho_s T_G + 2\rho_s (1+e)\alpha_s^2 g_0 T_G \tag{7}$$

where T_G is the granular temperature $\left[m^2.s^{-2}\right]$, e is the particle-particle restitution coefficient and g_0 is the radial distribution function. The first term on the right hand side of Equation 7 is the kinetic term and the second term is due to particle collisions. The granular temperature is associated with the kinetic energy of the

fluctuating particle motion and is introduced as:

$$T_G = \frac{1}{3}\vec{u}'^2 \tag{8}$$

where $\vec{u}'$ is the deviation of particle instantaneous velocity from mean particle velocity, like the Reynolds decomposition in turbulence modelling. In the derivation of Equation 8 it is assumed that deviations of particle velocity from mean velocity in all spatial directions are equal. It can be shown that the conservation equation for particle kinetic fluctuation energy reads [11]:

$$\frac{3}{2}\left[\frac{\partial}{\partial t}\left(\alpha_s \rho_s T_G\right) + \nabla\cdot\left(\alpha_s \rho_s \vec{u}_s T_G\right)\right] = \left(\bar{\tau}_s - p_s I\right):\nabla\vec{u}_s + \nabla\left(\kappa\nabla T_G\right) - \gamma - 3K_{gs}T_G \tag{9}$$

The first term on the right hand side is production of fluctuations by shear, the second term is diffusion of fluctuation energy, the third term is dissipation due to inelastic collisions, and the last term is dissipation by interaction with gas phase. According to Gidaspow et. al. [9] the diffusion coefficient for kinetic fluctuation energy is:

$$\kappa = \frac{150 d_s \rho_s \sqrt{T_G \pi}}{384(1+e)g_0}\left[1+\frac{6}{5}\alpha_s g_0 (1+e)\right]^2 + 2 d_s \rho_s \alpha_s{}^2 g_0 (1+e)\sqrt{\frac{T_G}{\pi}} \tag{10}$$

and collisional kinetic energy dissipation is represented by the expression derived by Lun et. al. [10]:

$$\gamma = \frac{12}{d_s\sqrt{\pi}}\rho_s \alpha_s{}^2 g_0 \left(1-e^2\right) T_G^{3/2} \tag{11}$$

The radial distribution function in Equations 7, 10 and 11 is a correction factor that modifies the probability of collisions between grains when the volume fraction of the solid phase increases up to its maximum value. A form successfully used by Ding and Gidaspow [20] is:

$$g_0 = \left[1 - \left(\frac{\alpha_s}{\alpha_{s,\max}}\right)^{1/3}\right]^{-1} \tag{12}$$

where $\alpha_{s,\max}$ is the maximum solid volume fraction or packing limit. For uniform spheres $\alpha_{s,\max} = \pi/3\sqrt{2}$ [11].

It can be seen in Equations 3 and 4 that momentum exchange between the gas and solid phase is based on the value of the interphase momentum exchange coefficient, K_{gs}. It can be written in the following general form:

$$K_{gs} = \frac{\alpha_g \alpha_s \rho_s f}{\tau_s} \tag{13}$$

where f is the drag function and is differently defined in the various momentum exchange coefficient models. τ_s is the particle relaxation time $[s]$ which is defined as

$$\tau_s = \frac{\rho_s d_s^2}{18\mu_g} \tag{14}$$

where d_s is the diameter $[m]$ of the granular material.

In the simulation of the KWB underfeed stoker furnace, the Syamlal-O'Brien [21] model was used to model the drag function:

$$f = \frac{\mathrm{Re}}{24v^2}\left(0.63 + \frac{4.8}{\sqrt{\mathrm{Re}/v}}\right)^2 \tag{15}$$

Re denotes the relative particle Reynolds number:

$$\mathrm{Re} = \frac{\rho_g \left|\vec{u}_s - \vec{u}_g\right| d_s}{\mu_g} \tag{16}$$

and v is called terminal velocity and is given by:

$$v = 0.5\left(A - 0.06T\,\mathrm{Re} + \sqrt{\left(0.06\,\mathrm{Re}\right)^2 + 0.12\,\mathrm{Re}\left(2B - A\right) + A^2}\right) \tag{17}$$

where

$$A = \alpha_g^{4.14} \tag{18}$$

$$B = \begin{cases} 0.8\alpha_g^{1.28} & \alpha_g \le 0.85 \\ \alpha_g^{2.65} & \alpha_g > 0.85 \end{cases} \tag{19}$$

Additionally, there are two parameters left in Equation 6 which need to be modelled: solid shear viscosity μ_s and solid bulk viscosity λ_s. The flow behaviour of the granular phase is determined by the solid stress tensor, particularly its viscosity terms. There are some equations to model the viscosity terms and in all of them they are proportional to the radial distribution function [9-13]. As it can be seen in Equation 12, by approaching the solid volume fraction to its maximum value (packing limit), the radial distribution function goes to infinity. Hence the bulk and shear viscosities calculated by these equations for packed bed condition tends to infinity, because the solid volume fraction is most of the time near the packing limit. Therefore, these models mostly provide unrealistic results for packed bed simulations. Moreover, it is worth to mention that the existing models for the bulk and shear viscosities are mainly assessed under fluidized bed conditions and by changing them the results are not valid anymore.

In this work, the viscosity terms are roughly determined by performing several simulations with different values for the bulk and shear viscosities, in order to obtain realistic simulation results concerning packed bed shape and flow behaviour qualitatively agreeing with observations.

2.2 Thermal conversion of particles

As mentioned, the second relevant part of fuel bed simulation is the thermal conversion of the particles. The modelling of particle thermal conversions is performed by the discrete phase model (DPM). In this study, as the first attempt, the standard combustible particle model of DPM is used to simulate particle thermal conversions based on the thermally thin particle assumption. This assumption neglects the intra-particle temperature gradient and simplifies the partial differential energy equation of the particles to the following ordinary differential equation [22]:

$$m_P c_P \frac{dT_P}{dt} = hA_p\left(T_\infty - T_P\right) + \varepsilon_P A_P \sigma\left(T_R^4 - T_P^4\right) + Q_S \tag{20}$$

where m_P, A_p, c_P and ε_P are mass $[kg]$, surface area $\left[m^2\right]$, heat capacity $\left[J.kg^{-1}.K^{-1}\right]$ and emissivity of the particle, respectively. h is the heat transfer coefficient $\left[W.m^{-2}.K^{-1}\right]$, T_∞ is ambient temperature $[K]$, σ is the Stefan-Boltzmann constant $\left[W.m^{-2}.K^{-4}\right]$, T_R is the radiation temperature $[K]$ and Q_S is the energy source/sink term $[W]$ originating from drying, pyrolysis

and char combustion processes.

The processes of particle thermal conversion are modelled by the available DPM sub-models for drying, pyrolysis and char burnout. Drying is modelled by two subsequent steps, according to the vaporisation law and the boiling law of the DPM.

The vaporisation law is applied when the particle temperature is between the vaporisation temperature and boiling temperature. The vaporisation temperature is a model parameter and has no physical significance. The rate of vaporisation is governed by diffusion and it is related to the difference in vapour concentrations at the particle surface and bulk gas as well as the mass transfer coefficient which is calculated from the Sherwood number. Afterwards the particle temperature is updated according to the Equation 20 and replacing the following sink term:

$$Q_S = -\dot{m}_{vap} h_{fg} \tag{21}$$

where $\dot{m}_{vap}$ is the vaporisation rate $\left[kg.s^{-1}\right]$ and h_{fg} is the latent heat $\left[J.kg^{-1}\right]$.

Once the particle temperature reaches the boiling temperature, the boiling law is initiated. Throughout the boiling law, the temperature of the particle is assumed to remain constant at boiling temperature. Hence, the boiling rate is limited by the heat transfer rate and derived from Equation 20:

$$\dot{m}_{boil} h_{fg} = hA_p \left(T_\infty - T_P\right) + \varepsilon_P A_P \sigma \left(T_R^4 - T_P^4\right) \tag{22}$$

where $\dot{m}_{boil}$ is the boiling rate $\left[kg.s^{-1}\right]$.

Several models for biomass pyrolysis are reported in the literatures. There is not a meaningful difference between their results under the combustion conditions where the heating rate is high. Therefore, in this study in order to decrease the computational effort a simple and sufficiently accurate pyrolysis model was applied. The mechanism of the pyrolysis reaction considered to be single-step and the release rate of the volatiles assumed to be first order depending on the amount of volatiles remaining in the particle,

$$\dot{m}_{py} = -k\left[m_p - \left(1-Y_{v,0}\right)\left(1-Y_{w,0}\right)m_{p,0}\right] \tag{23}$$

where $Y_{v,0}$, $Y_{w,0}$ and $m_{p,0}$ are volatile fraction, water fraction and mass of the particle at initial condition, respectively. The kinetic rate of this single-step reaction, k, is calculated from an Arrhenius equation:

$$k = A\exp\left(-\frac{E}{RT}\right) \tag{24}$$

A is the pre-exponential factor and E is the activation energy. $A = 2.5\times10^8\ [s^{-1}]$ and $E = 125\ [kJ.mol^{-1}]$ are used for the simulation of the KWB underfeed stoker furnace [23]. Because these values are for the pyrolysis of softwood and the fuel in the KWB underfeed stoker furnace is softwood pellets. The temperature of the particle during the pyrolysis is calculated from Equation 20. The heat of pyrolysis reaction is neglected in comparison with heat of drying and combustion reactions [23, 24].

After the volatiles of the particle are completely released, the char oxidation surface reaction starts to consume the char of the particle. The product of this heterogeneous reaction was assumed to be carbon monoxide. This assumption is justified by the equilibrium of the Boudouard heterogeneous reaction, because at particle temperatures under combustion conditions mainly carbon monoxide is released during char burnout [25]. The rate of the char burnout reaction is assumed to be diffusion limited, such as in several studies [26-29]. According to the fact that the oxygen mass is conserved in the particle boundary layer, i.e. quasi-steady state assumption, the char oxidation rate is derived by assuming that the oxygen consumption at the particle surface is equal to the diffusion of oxygen across the particle boundary layer. The mass transfer rate of the oxygen from the bulk to the surface of the particle is obtained from the Sherwood number. It can be shown that in the DPM standard diffusion limited char burnout model, a constant Sherwood number equal to 2.0 is assumed. The Sherwood number equal to 2.0 is valid only for the stagnation conditions where the particle-gas relative velocity is equal to zero. Therefore, for the cases with the significant particle-gas relative velocity, as for the KWB underfeed stoker furnace, this model underpredicts the rate of char oxidation. Because it neglects the effect of the particle-gas relative velocity on the oxygen mass transfer from the bulk to the surface of the particle.

In order to overcome this shortcoming, the following equation was applied for the char burnout rate:

$$\dot{m}_{comb} = -2\pi d_p \mathrm{Sh} D_{AB} \frac{Y_{o2} T_\infty \rho_g}{s\left(T_p + T_\infty\right)} \tag{25}$$

where $\dot{m}_{comb}$ is the char burnout rate $\left[kg.s^{-1}\right]$, D_{AB} is the binary diffusion coefficient $\left[m^2.s^{-1}\right]$, Y_{o2} is the bulk oxygen mass fraction, s is the ratio between mass of oxygen to the mass of char in the char oxidation reaction and Sh is Sherwood number calculated from Ranz-Marshall correlation [30]:

$$\mathrm{Sh} = 2 + 0.6\,\mathrm{Re}^{1/2}\,\mathrm{Sc}^{1/3} \tag{26}$$

where Sc is the Schmidt number and Re is the Reynolds number based on the particle-gas relative velocity, see Equation 16.

It can be assumed that during the char burnout reaction the particle-gas relative velocity and flue gas temperature are nearly constant. Therefore, the average particle-gas relative velocity and flue gas temperature during the char oxidation reaction, obtained form the simulations, are used to calculate the Reynolds and Schmidt numbers in the Sherwood number correlation. This modification leads to an improvement of the prediction accuracy concerning char burnout rate, since it provides a more realistic description of the mass transfer coefficient than the standard DPM model.

3 INVESTIGATED GRATE SYSTEM

The grate of the KWB underfeed stoker furnace is shown in Figure 1. The fuel, softwood pellets, is fed on the grate from below and is transported towards the outer edge of the grate. Primary air is supplied through the grate from nozzles at the bottom which form a concentric ring with the fuel feeding tube in the centre. In the simulation the primary air nozzles are represented by three concentric rings as it is shown in Figure 1.

Since wood pellets are a very homogeneous biomass fuel, it is realistic to assume an average biomass size and physical properties to characterise them. Therefore, in the Euler-Granular model the solid phase was represented

only by one particle size class, i.e. one solid phase. As it mentioned before, it considerably reduces the calculation time. Moreover, the pellets are assumed to have spherical forms and their average diameter is calculated based on the equivalent volume. The fuel analysis and operating conditions and other input parameters used in the simulation of the KWB underfeed stoker grate furnace are listed in Table I.

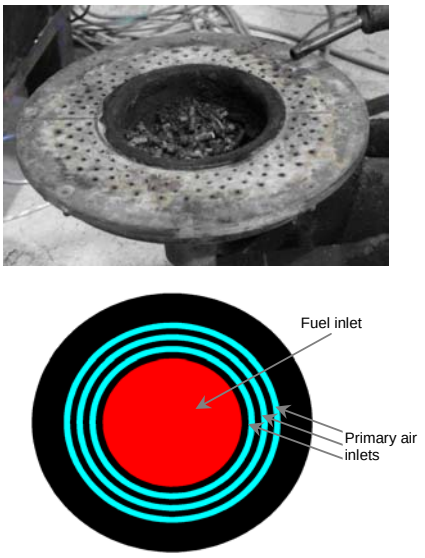

Figure 1: Top: grate of the KWB underfeed stoker furnace; bottom: scheme of the grate used for simulations

Table I: Fuel analysis, operating conditions and particle physical properties used in the simulation

Ultimate Analysis		
C	wt% d.b.	50.1
H	wt% d.b.	5.7
O	wt% d.b.	43.72
N	wt% d.b.	0.12
Ash	wt% d.b.	0.36
Proximate Analysis		
Moisture content	wt% w.b.	8.12
Volatiles	wt% d.b.	77.1
Fixed carbon	wt% d.b.	22.54
Net calorific value	MJ/kg w.b.	17.244
Total air ratio	-	1.58
Primary air ratio	-	0.64
Particle Physical Properties		
Average diameter	mm	6
Average density	$kg.m^{-3}$	1120
Specific heat	$J.kg^{-1}.K^{-1}$	1500 + T
Thermal conductivity	$W.m^{-1}.K^{-1}$	0.173

Since the plant technology investigated is restricted Know-How of the company KWB-Kraft und Wärme aus Biomasse GmbH, only selected results, relevant concerning 3D packed bed combustion model development, are presented in the next part.

4 RESULTS AND DISCUSSION

The positions of the drying, pyrolysis, and char burnout zone inside the fuel bed are illustrated in Figure 2, Figure 3 and Figure 4, respectively by means of the particle tracks on the grate coloured by drying, pyrolysis and char burnout rates as well as the contours of these rates along a vertical cross section through the grate axis. As it is shown in these figures, the three sub-processes of particle thermal conversion sequently happen with an overlap between each other. Drying takes place in the centre of the bed above the fuel inlet. Afterwards particles start to release volatiles along their radial path to the outer edge of the grate. According to the simulation, the main part of the pyrolysis happens at a ring around the drying zone. The remaining char mainly reacts with oxygen above the outer primary air injection region.

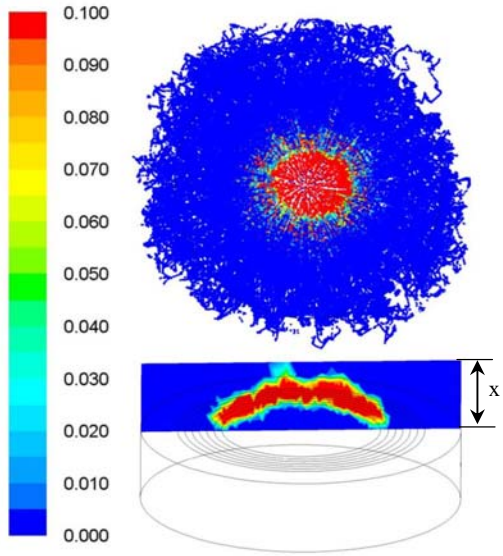

Figure 2: Top: particle tracks on the grate coloured by drying rates [mg/s]; bottom: contours of drying rate [mg/s] at a vertical cross section through the grate axis; x= 5cm

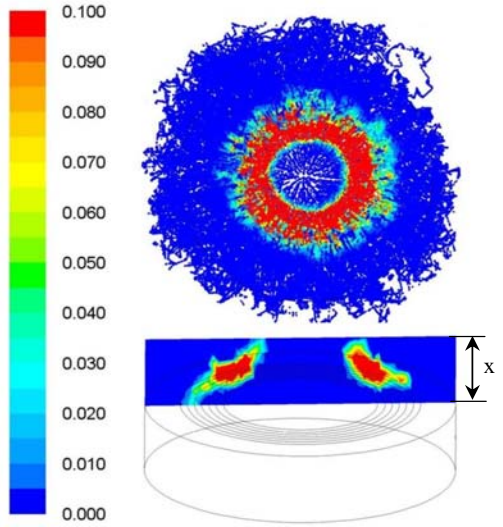

Figure 3: Top: particle tracks on the grate coloured by pyrolysis rates [mg/s]; bottom: contours of pyrolysis rate [mg/s] at a vertical cross section through the grate axis; x= 5cm

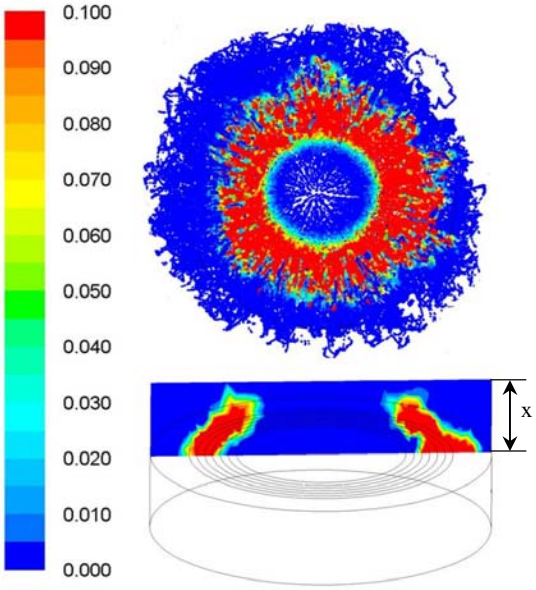

Figure 4: Top: particle tracks on the grate coloured by char burnout rates [mg/s]; bottom: contours of char burnout rate [mg/s] at a vertical cross section through the grate axis; x= 5cm

The particle tracks coloured by the simulated particle temperatures are shown in Figure 5. The flue gas temperatures along the vertical cross section of the combustion chamber as well as a horizontal cross section close to the surface of the fuel bed are shown in Figure 6. Additionally, a picture taken from a window at the top of the furnace is enclosed in Figure 6 for comparison. However, from the picture the entire bed can not be seen, due to a reduction of diameter at the position where the secondary air is injected.

The predicted locations of the fuel conversion stages in the fuel bed are an explanation of the simulated particle temperatures in Figure 5 and also the flue gas temperatures along the horizontal cross section close to the surface of the fuel bed in Figure 6. It can be seen, that at the surface of the fuel bed, the lowest particle and flue gas temperatures occur in the centre, which is due to the fact that drying takes place there. After the drying region the particle temperatures increase due to radiation and the volatile components of the particles are released. A fraction of the volatile components burns at the surface of the fuel bed, therefore the flue gas temperatures along the horizontal cross section shown in Figure 6 have their highest value right above the pyrolysis region. The highest particle temperatures occur at the outer primary air inlet region due to char oxidation. Outside the primary air injection rings, both the flue gas and particle temperatures are reduced, because almost no homogeneous gas phase reactions happen in this region and also the energy release due to char burnout is low due to the comparatively small amount of char. The results regarding to the variations of the particle temperatures, Figure 5, and the flue gas temperatures along the horizontal cross section close to the surface of the fuel bed, Figure 6, are in good agreement with the picture taken from the top of the furnace, shown in Figure 6.

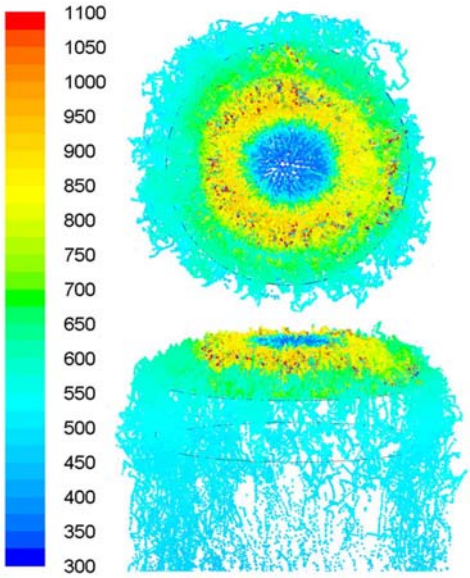

Figure 5: Particle tracks on the grate coloured by particle temperatures (K)

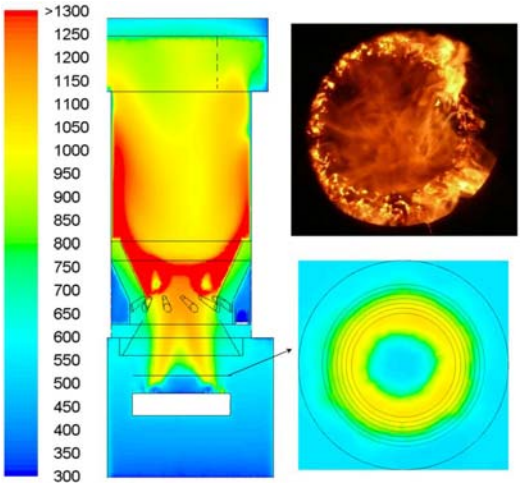

Figure 6: Contours of flue gas temperatures (K); left: along the vertical cross section of the combustion chamber; right top: visual observation from a window at the top of the furnace; right bottom: along a horizontal cross section close to the surface of the fuel bed (4cm above the grate, shown in the vertical cross section)

In Figure 7 to Figure 10 the contours of O_2, H_2O, CH_4, and CO close to the surface of the fuel bed are shown, respectively. The distribution of these species can be explained by the positions of the thermal conversion sub-processes. These figures pronounce that the release profiles of the species from the fuel bed are dependent on the radial as well as angular positions on the grate. Hence, modelling the release of volatile components from the fuel bed to the gas phase with 1D profiles as the boundary conditions for the gas phase simulation may lead to some inconsistencies.

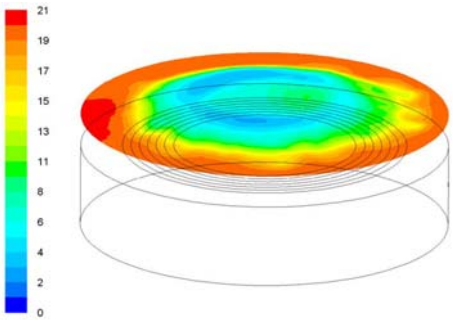

Figure 7: Contours of O_2 concentrations approximately at the surface of the fuel bed [vol%-dry]

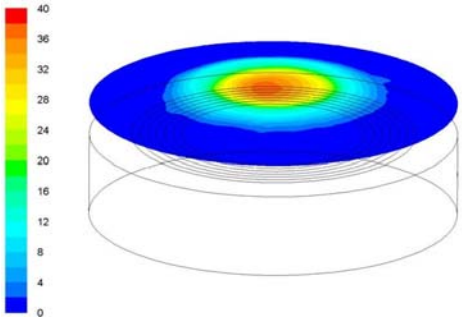

Figure 8: Contours of H_2O concentrations approximately at the surface of the fuel bed [vol%]

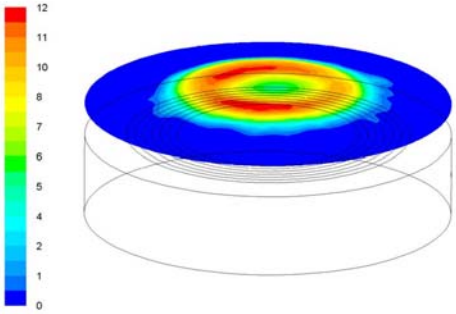

Figure 9: Contours of CH_4 concentrations approximately at the surface of the fuel bed [vol%-dry]

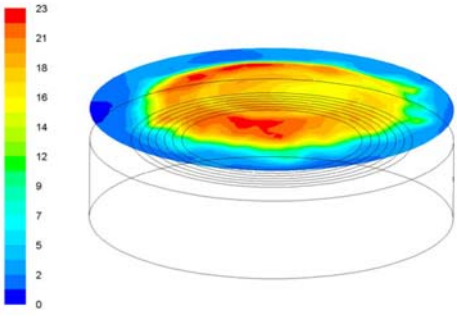

Figure 10: Contours of CO concentrations approximately at the surface of the fuel bed [vol%-dry]

5 CONCLUSIONS

In order to design and optimise biomass grate furnaces, a CFD based packed bed combustion model has been developed. The model is based on the kinetic theory of granular flow for the prediction of the hydrodynamics of the packed bed and the thermally thin particle model with a set of sufficiently accurate transient models for the thermal conversion of individual biomass particles. The thermal conversion of the entire bed is simulated by predicting the trajectories and the thermal conversion of the particles in the bed.

The model has been successfully applied to simulate KWB underfeed stoker grate furnace. The maximum predicted particle temperatures in the bed are relatively lower than the previous experiments of a lab-scale batch reactor. It implies that the products of the char oxidation reaction can not be only carbon monoxide and a fraction of carbon monoxide should also be considered. However, the modified char burnout model predicts the unburned char to be less than 1 wt.%, which is in good agreement regarding the burnout quality of the grate ash. Moreover, the results regarding variations of the particle and flue gas temperatures at the bed surface and the locations of the fuel conversion stages are in qualitative agreements with visual observations of the packed bed.

Hence, the new 3D packed bed model provides the following advantages for the simulation of grate furnaces:

- The effect of particle related parameters, e.g. size, physical properties and chemical compositions, on the thermal conversion of the entire packed bed can be investigated
- Modelling the hydrodynamics of the packed bed by the granular kinetic theory allows to model the particle movements on the grate under consideration of particle-particle collisions
- The applied hydrodynamics model allows to study the influence of grate motion and primary air distribution below the bed on the particle trajectories
- The influence of primary air distribution on the thermal conversion of the packed beds can be investigated
- Better prediction of the profiles of species and energy released from the fuel bed, as important input data for the simulation of gas phase combustion.

As next steps of model improvement, the development of an enhanced heat transfer model for the packed bed, the utilisation of a thermally thick model for particle conversion and the application of a new hybrid Euler-Euler/Euler-Lagrange model for the coupled simulation of particle movement and thermal conversion are foreseen.

6 REFERENCES

[1] Scharler R., Fleckl, T., Obernberger, I, 2003: Modification of a Magnussen Constant of the Eddy Dissipation Model for biomass grate furnaces by means of hot gas in-situ FT-IR absorption spectroscopy. Progress in Computational Fluid dynamics, Vol. 3, pp. 102-111.

[2] Scharler R., Obernberger I., 2000: Numerical optimisations of biomass grate furnaces.

Proceedings of the 5th European Conference on Industrial Furnaces and Boilers INFUB, Portugal.
[3] Scharler R., Zahirovic S., Schulze K., Kleditzsch S. Obernberger I., 2006: Simulationsgestützte Auslegung und Optimierung von Biomassefeuerungs- und Kesselanlagen – Einsatzmöglichkeiten, Stand der Technik und innovative Methoden. Österreichische Ingenieur- und Architektenzeitung, Vol. 10-12, pp. 296-309.
[4] Scharler, R., 2001: Entwicklung und Optimierung von Biomasse-Rostfeuerungen durch CFD-Analyse. Ph.D. thesis, Graz University of Technology, Austria.
[5] Dziugys A., Peters B., 2001: An approach to simulate the motion of spherical and non-spherical fuel particles in combustion chambers. Granular Matter, Vol. 3, pp. 231-265.
[6] Cundall P. A., Strack O. D. L., 1979: Discrete numerical model for granular assembelies. Geotheqnique, Vil. 29, 47-65.
[7] Hoomans B. p. B., Kuipers J. A. M. Briels W. J. van Swaiij W. P. M., 1996: Discrete particle simulation of bubble and slug formation in a two-dimensional gas fluidized bed: a hard sphere approach, Chemical Engineering Science, Vol. 51, pp. 99-118.
[8] Hjertager B. H., Solberg T., Ibsen C. H., Hansen K. G., 2003: Multi-Fluid CFD modelling of fluidised bed reactors. Invited Presentation Computational Fluid Dynamics in Chemical Engineering III, Davos, Switzerland.
[9] Gidaspow D., Bezburuah R., Ding J., 1992: Hydrodynamics of Circulating Fluidized Beds, Kinetic Theory Approach. In O. E. Potter and D. J. Nicklin, Eds., Fluidization VII, Engineering Foundation, pp. 75-82.
[10] Lun C. K. K., Savage S. B., Jeffrey D. J., Chepurniy N., 1984: Kinetic theories for granular flow: inelastic particles in Couette flow and slightly inelastic particles in a general flow field. J. Fluid Mech., Vol. 140, pp. 223–256.
[11] Gidaspow D., 1994: Multiphase flow and fluidization. Academic Press, Boston.
[12] Syamlal M., Rogers W., O'Brien T. J., 1993: MFIX Documentation: Volume 1, Theory Guide. National Technical Information Service, Springfield, VA, DOE/METC-9411004, NTIS/DE9400087.
[13] Gidaspow D., Jayaswal U. K., Ding J., 1991: Navir-Stokes Equation Model for Liquid-Solid Flows Using Kinetic Theory. Liquid Solid Flows, Vol. 118, New York: ASME, pp. 165-178.
[14] Sinclair J. L., Jackson R., 1989: Gas–particle flow in a vertical pipe with particle–particle interactions. AIChE Journal, Vol. 35, pp. 1473–1486.
[15] Chapman S., Cowling T.G., 1970: The mathematical theory of non-uniform gases. Cambridge University Press, Cambridge.
[16] Wang W., Lu B., Zhang N., Shi Z., Li J., 2010: A review of multiscale CFD for gas–solid CFB modelling. Int J Multiphase Flow, Vol. 36, pp. 109-118.
[17] Taghipour F., Ellis N., Wong C., 2005: Experimental and computational study of gas–solid fluidized bed hydrodynamics. Chemical Engineering Science, Vol. 60, pp. 6857-6867.
[18] Boemer, A., 1996: Euler/Euler-Simulation der Fluiddynamik blasenbildender Wirbelschichten. PhD Thesis, University of Aachen, Germany.
[19] Popoff B., Braun M., 2007: A Lagrangian Approach to Dense Particulate Flows. 6th International Conference on Multiphase Flow (ICMF), Leipzig, Germany.
[20] Ding J., Gidaspow D., 1990: A Bubbling Fluidization Model Using Kinetic Theory of Granular Flow. AIChE J., Vol. 36, pp. 523–538.
[21] Syamlal M., O'Brien T. J., 1989: Computer Simulation of Bubbles in a Fluidized Bed. AIChE Symp. Series, Vol. 85, pp. 22-31.
[22] ANSYS FLUENT 12.0, Theory Guide.
[23] Gronli M., 1996: A theoretical and experimental study of the thermal degredation of biomass. Ph.D. thesis, The Norwegian University of Science and Technology, Norway.
[24] Zahirovic S., Scharler R., Obernberger I., 2004: Advanced CFD modelling of pulverised biomass combustion. Proceeding of the 6th International Conference Science in Thermal and Biomass Conversion, Victoria, Canada, Vol. 1, pp. 267-284.
[25] Mathieu P., Dubuisson R., 2002: Performance analysis of a biomass gasifier. Energy Conversion and Management, Vol. 43, pp. 1291–1299.
[26] Bruch C., Peters B., Nussbaumer T., 2003: Modelling wood combustion under fixed bed combustion. Fuel, Vol. 82, pp. 729-738.
[27] Wu C., 2006: Fuel-NOx formation during low-grade fuel combustion in a swirling-flow burner. Ph.D thesis, Brigham Young University, USA.
[28] Porteiro J., Miguez J. L., Granada E., Moran J. C., 2006: Mathematical modelling of the combustion of a single wood particle. Fuel Processing Technology, Vol. 87, pp. 169-175.
[29] Meesri C., Moghtaderi B., 2003: Experimental and numerical analysis of sawdust-char combustion reactivity in a drop tube reactor. Combustion Science and Technology, Vol. 175, pp. 793-823.
[30] Bird R. B., Stewart W. E., Lightfoot E. N., 2002: Transport phenomena, John Wiley & Sons.

7 ACKNOWLEDGEMENTS

We gratefully acknowledge the Austrian K*plus* program of the Federal Government of Austria, the State Government of Styria as well as the State Government of Lower Austria for funding the work presented in this paper.

8 LOGO SPACE

BIOENERGIESYSTEME GmbH
Inffeldgasse 21b, A-8010 Graz